Dielectric response of isolated carbon nanotubes investigated by spatially resolved electron energy-loss spectroscopy: From multiwalled to single-walled nanotubes

O. Stéphan,[1,*] D. Taverna,[1] M. Kociak,[1] K. Suenaga,[2] L. Henrard,[3] and C. Colliex[1]

[1]*Laboratoire de Physique des Solides, Associé au CNRS, Bâtiment 510, Université Paris-Sud, 91405 Orsay, France*

[2]*JST-ICORP, Department of Physics, Meijo University, Nagoya 468-8502, Japan*

[3]*Laboratoire de Physique du Solide, Facultés Universitaires Notre-Dame de la Paix,*

61 rue de Bruxelles, 5000 Namur, Belgium

To investigate the dielectric response of isolated single-walled carbon nanotubes, (SWCNTs), spatially resolved electron energy-loss spectroscopy measurements have been carried out using a scanning transmission electron microscope in a near-field geometry. Spectra have been compared with those acquired on multiwalled carbon nanotubes (MWCNTs) made of different numbers of layers, and with simulations performed within the framework of the continuum dielectric theory, taking into account the local anisotropic character of these nanostructures and adapted to the cylindrical geometry. Experimental data show a dispersion of mode energies as a function of the ratio of the internal and external diameters, as predicted by the continuum dielectric model. For thin MWCNTs, two polarization modes have been identified at 15 and 19 eV, indexed as tangential and radial surface-plasmon modes, respectively, resulting from the coupling of the two surface modes on the internal and external surfaces of the nanotubes. We finally show that the dielectric response of a SWCNT, displaying a single energy mode at 15 eV, can be understood in the dielectric model as the thin layer limit of surface-plasmon excitation of MWCNTs.

I. INTRODUCTION

Optical properties of nanoparticles and nanostructured materials nowadays constitute a very exciting field of investigation for applications, such as the realization of integrated optical circuits. Many recent efforts concern the wave guiding of subwavelength excitations in the surface polariton band-gap material,[1] the development of photonic band-gap devices in the visible domain,[2] or the possibility of tuning the plasmon frequency of nanostructured materials.[3] In such a context, a detailed understanding of the plasmon excitation modes of isolated nanostructures, as well as their evolution and coupling when nanostructures form arrays, is of prime interest. Among nanostructures, anisotropic nanoparticles have been less extensively studied. So far, dielectric models for locally anisotropic nanospheres[4–6] and isotropic nanocylinders[7,8] have been proposed and experimentally validated.[9,10] We have therefore extended the dielectric model to anisotropic cylinders[11] and first numerical data are used in the present contribution in order to interpret our experimental data.

In a recent paper, we have analyzed the electrostatic limit of the surface-plasmon coupling of thin and thick anisotropic WS$_2$ nanocylinders.[12] We have concluded that in the very thin shell limit, the two collective surface modes occurring from the coupling between the internal and external surfaces of the hollow cylinder can be indexed as a tangential (symmetric) and a radial (antisymmetric) mode as defined in the isotropic case. Moreover, each mode can be separately associated with a specific component of the dielectric tensor of the corresponding lamellar WS$_2$ bulk material.[12]

In the present paper, we show that electron energy-loss spectroscopy (EELS) measurements in a near-field geometry[13] in a scanning transmission electron microscope (STEM) can be used to measure the dielectric response of individual carbon nanotubes made of a well-defined number of layers down to a single one. We show that the dielectric response of a single-walled carbon nanotube (SWCNT) is characterized (besides the π plasmon) by an isolated mode at 15 eV. Although reported previously in the literature,[14,15] this mode has not been interpreted so far. By comparing the dielectric response of a SWCNT with that of multiwalled carbon nanotubes (MWCNTs) made of different numbers of layers, we show that this single mode is well understood as a limiting case of surface-plasmon modes of MWCNTs when only the tangential mode remains. Beyond the interpretation of this spectrum, we validate one of the major predictions of the dielectric theory, i.e., the r/R ratio dependence (where r and R are, respectively, the inner and outer radii of the nanotubes) of the energy position of the surface-plasmon excitations in hollow nanoparticles. We also point out the counterintuitive result that in this situation the notion of dielectric continuum remains relevant for the description of such a tiny object (SWCNT) made up of a monoatomic layer.

II. EXPERIMENTS AND SIMULATIONS

SWCNT samples were synthesized by arc discharge as described in Ref. 16. MWCNTs were synthesized by chemical vapor deposition as described in Ref. 17. They exhibit the peculiarity of being made up of a very small number of layers, typically from two to six. It corresponds to the ideal morphology for evidencing surface-plasmon coupling in hollow cylinders.

EELS measurements were performed in a STEM VG HB501 with a field-emission gun operated at 100 keV and fitted with a Gatan 666 parallel-EELS spectrometer. Such a
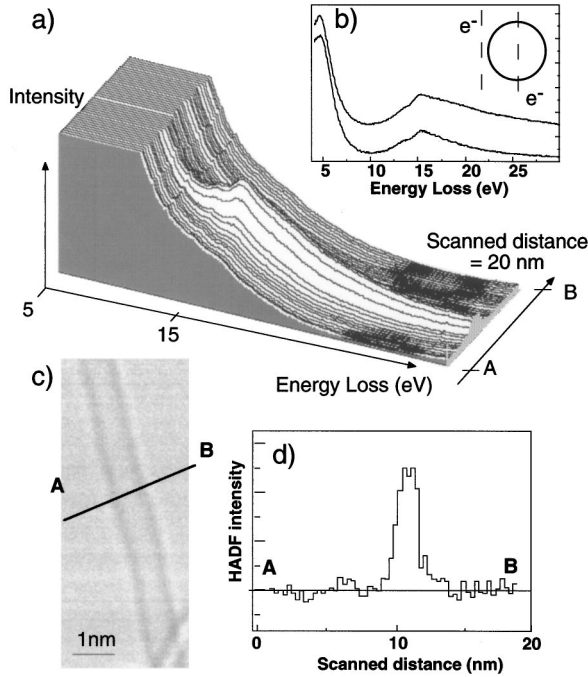
FIG. 1. (a) Series of EELS spectra acquired while scanning the STEM probe across an isolated SWCNT. (b) Two spectra for penetrating (top) and nonpenetrating (bottom) geometry. (c) Bright field image. (d) HADF profile.

STEM instrument delivers a 0.5-nm electron probe of high brightness for local analysis at the nanometer scale. EELS spectra were recorded with a charge-coupled device camera optically coupled[18] to a scintillator in the imaging plane of a Gatan magnetic sector. The specificity of a STEM is to provide multisignal detection from a nanovolume of analysis. In these experiments, a high angle annular dark field (HADF) detector has been used, for simultaneous dark field imaging in parallel with the EELS analysis. This imaging mode is very useful when applied to nanotubes, because of the simple interpretation of the recorded contrast. Indeed, the signal intensity is directly proportional to the projected mass.[19] In the case of simple objects, straightforward information on their topography and morphology can then be extracted. In the present study, HADF profiles have been exploited to determine the values of the inner and outer radii r and R of the investigated nanotubes. For nanotubes made of a small number of layers (less than three), bright field images were also recorded for improving the nanotube structural parameters identification.

We have operated the STEM in the so-called "spectrum imaging" mode,[20,21] which consists of acquiring spectroscopic information (in our case combined with topographic information) for every position of the subnanometer probe, typically of 0.5-nm diameter, as it is scanned along a predefined line across the selected nano-object. Figure 1(a) shows an example of such a spatially resolved EELS experiment on a SWCNT. The beam was scanned from vacuum at a large impact parameter (the impact parameter is defined as the distance between the electron probe position and the axis of the nanotube) to the center of the nanotube, with spatial increments of 0.25 nm. Note that in this case the signal is

well sampled, the step size being about half the probe size. Each individual spectrum was recorded with a 0.4-s acquisition time and a 0.5-eV resolution. An unambiguous identification of the impact-parameter value was made possible by the simultaneous acquisition of the HADF profile. Specific spectra corresponding to grazing incidence, or to penetrating or nonpenetrating geometry, can then be discriminated. The HADF profile [Fig. 1(d)], a bright field image [Fig. 1(c)], as well as two selected EELS spectra for a penetrating and a nonpenetrating geometry [Fig. 1(b)] are also shown.

For studying surface-plasmon modes on isolated nanotubes, we have selected spectra recorded in a nonpenetrating geometry for which no contribution of bulk modes is expected. From a classical point of view, for nanotubes as well as for all nanoparticles, the measured energy loss can be understood as follows: an electron traveling along the particle aloof a classical trajectory excites its surface dielectric modes, which gives rise to an induced field acting back on the electron and therefore responsible for a given energy loss. The electromagnetic response of such nanoparticles is described by their response function $\gamma_Q(\omega)$ (where Q is the momentum transfer), which is defined as the proportionality coefficient connecting the induced electric potential to the external applied one. Particularly, in the case of tubular nanoparticles, the momentum transfer decomposes into a component parallel to the direction of the tube axis (k_z component) and an angular component ($m\hbar$ component). Due to the symmetry of the problem, m takes discrete integer values, while k is a continuous variable. The surface-plasmon excitations are described in terms of resonances in the response function. More specifically, in a nonpenetrating geometry and for a given impact parameter b, the EELS spectrum can be expressed as

$$P_{m,k}(\omega,b) = \sum_m \int dk\, C_{m,k}(\omega,b) \mathrm{Im}[\gamma_{m,k}(\omega)],$$

where $C_{m,k}(\omega,b)$ is a kinematical factor depending on the experimental conditions (impact parameter, momentum transfer, and acceleration voltage). At large impact parameters b, $C_{m,k}(\omega,b)$ decreases exponentially with b. Thus, as we probe in such a nonpenetrating geometry the evanescent electromagnetic field decaying from the surface of the nanoparticle into vacuum, these measurements are also referred to as near-field EELS spectroscopy[13] measurements.

In order to interpret our data, we have performed the EELS spectra simulation within the nonretarded continuum dielectric model. This approach has been developed so far for spherical anisotropic particles.[6] EELS spectra simulation in this spherical geometry has already proved to give a good agreement with experimental near-field EELS data on carbon nanotubes and onions.[9] In order to better account for the object geometry, simulations based on an extension of this model to cylindrical geometry are presented. Therefore, these simulations account for both an accurate description of the dielectric properties of the constitutive material (via the continuum dielectric model and the dielectric tensor of graphite) and the exact cylindrical geometry of the experiment. A detailed description of the analytical and computa-
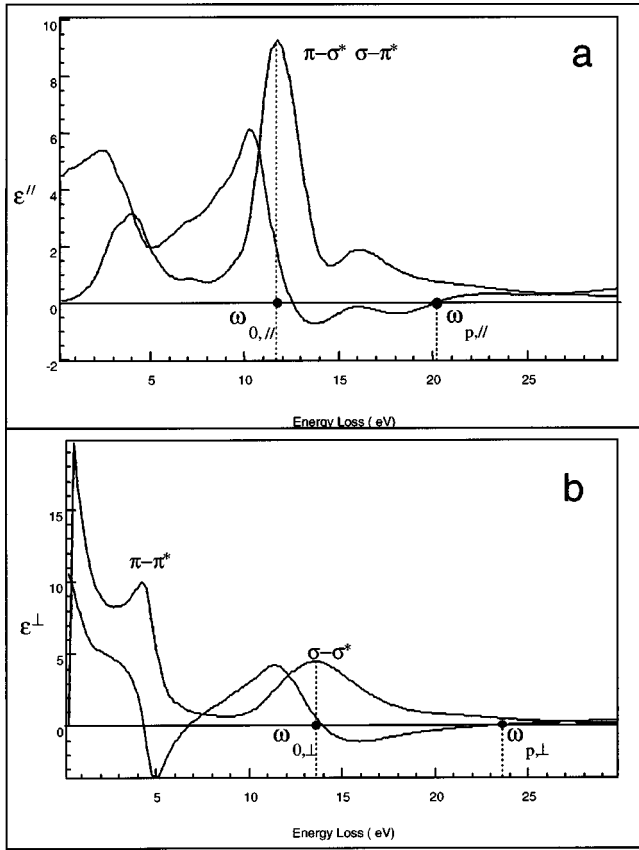
FIG. 2. The dielectric tensor of graphite, as compiled by Draine (Ref. 21). The real and imaginary parts of each component are displayed, respectively, with solid and dashed lines.

FIG. 3. Experimental EELS spectra recorded at grazing incidence on C nanotubes with different r/R ratios. (a) Spectra subtracted from the elastic peak by spatial difference. (b) Second derivative mode in the energy range 10–30 eV.

tional details can be found in Ref. 11. The starting hypothesis of the continuum dielectric model is that the response function of the nanoparticle is obtained using the local bulk dielectric properties of the material constituting the nano-object. The nanotube is then considered as a hollow nanocylinder made of a continuous medium, consistent with the fact that the transferred wavelength is very long as compared to the interatomic distance in graphite lattice. Here, as we are dealing with C nanotubes, the input dielectric constant for the simulation was introduced through tabulated values obtained from compiled optical and EELS measurements on graphite[22] (see Fig. 2). Because graphite is an anisotropic material, a tensorial description of the dielectric properties is necessary. We define the anisotropy axis **c** as the axis perpendicular to the basal planes. Then, $\varepsilon_\perp$ corresponds to the tensor component associated with the response for a momentum transfer perpendicular to this **c** axis. The excitations associated with $\varepsilon_\perp$ will also be named in-plane excitations. Similarly, $\varepsilon_\parallel$ is the component associated with a momentum transfer parallel to the **c** axis, referred to as out-of-plane excitations. Finally, the specificity of carbon nanotubes, which constitute cylindrical locally anisotropic particles, is to require an adapted extension of this macroscopic theory: the dielectric tensor is then expressed as a tensor locally diagonal in cylindrical coordinates.[11] This procedure is similar to that previously used for spherical geometry.[4,9]

III. RESULTS AND DISCUSSION

A. General features

In the following, an interpretation for the near-field EELS spectrum of a SWCNT is put forward. It issues from a detailed analysis of spectra recorded on a collection of individual C nanotubes with different numbers of layers and r and R values where r and R are defined for MWCNTs as the internal and external radii, respectively.

Figure 3(a) shows near-field EELS spectra acquired at grazing incidence for different C nanotubes made of one to five coaxial graphene layers and the second derivative of the spectra are shown in Fig. 3(b). The r/R ratio values reported on the figures increase from top to bottom. For SWCNTs, an estimation of the r/R value is not straightforward. As labeled in Fig. 3, this ratio is approximated by taking the limit $r/R \rightarrow 1$. This point will be discussed more extensively later in the text. The signals in the normal mode are subtracted from the zero loss peak by spatial difference (the spectrum detected when the probe passes through empty space far from the nanotube, where no loss is expected, is subtracted from the spectrum of interest, after normalization). The second derivative mode was calculated *a posteriori* as a second dif-
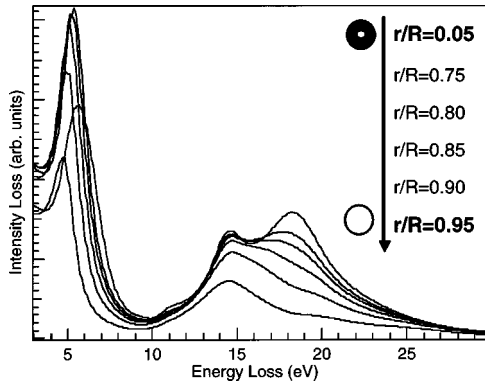
FIG. 4. Simulation of EELS spectra at grazing incidence of carbon nanotubes with external radius $R = 20$ nm and variable internal radius r. From top to bottom, spectra computed for setting, respectively, the radius ratio r/R to 0.05, 0.75, 0.80, 0.85, 0.90, and 0.95.

ference of normal spectra. This data processing is useful for a clear identification of the different energy modes. However, relative intensities in the second derivative curves are then meaningless.

All spectra exhibit two well-separated groups of large resonances. The sharpest resonance centered on 5–6 eV is attributed to excitations of π electrons while the broader one above 10 eV implies π- and σ-electron excitations. Since the π-plasmon excitations are partly blurred by the no-loss peak and since they are less sensitive to the tube morphology, our analysis focuses on the features appearing above 10 eV.

B. Effect of the r/R ratio

Analyzing Fig. 3, for $r/R < 0.5$, the spectrum is very similar to that recorded on large MWCNTs (typically made up of 10 to 30 shells with r/R values of 0.1–0.2) with two major peaks centered at 15 and 17 eV and with a shoulder at 12 eV.[9] When the r/R ratio increases, i.e., $(0.65 < r/R < 0.73)$, the two major modes merge progressively, and the high-energy mode intensity decreases. Then, for a single layer with $R = 6$ Å, one single mode remains at 15 eV while a weak shoulder is observed at 19 eV. Note that, in this limit case, a redefinition of r/R is necessary and is based on the arbitrary choice of the effective dielectric thickness. We believe that a pertinent estimation of this thickness is of the order of 1 Å, which is roughly the order of magnitude of the p_z orbital expansion. If we consider the same effective thickness for both SWNTs, the r/R ratio will be closer to one as the tube radius increases.

The corresponding simulated spectra are gathered in Fig. 4. Good agreement is found with the general trends exhibited in the experimental data described earlier and the SWCNT spectrum is well reproduced for the limit of r/R values close to 1. More specifically for SWCNTs, the difference between the tube with $R = 6$ and $R = 11$ Å is also quantitatively reproduced. The tube with $R = 11$ Å (and an effective dielectric thickness of approximately 1 Å) is very similar to simulations obtained for r/R very close to 1, i.e., 0.95, while the tube with $R = 6$ Å presents an important shoulder at 19 eV
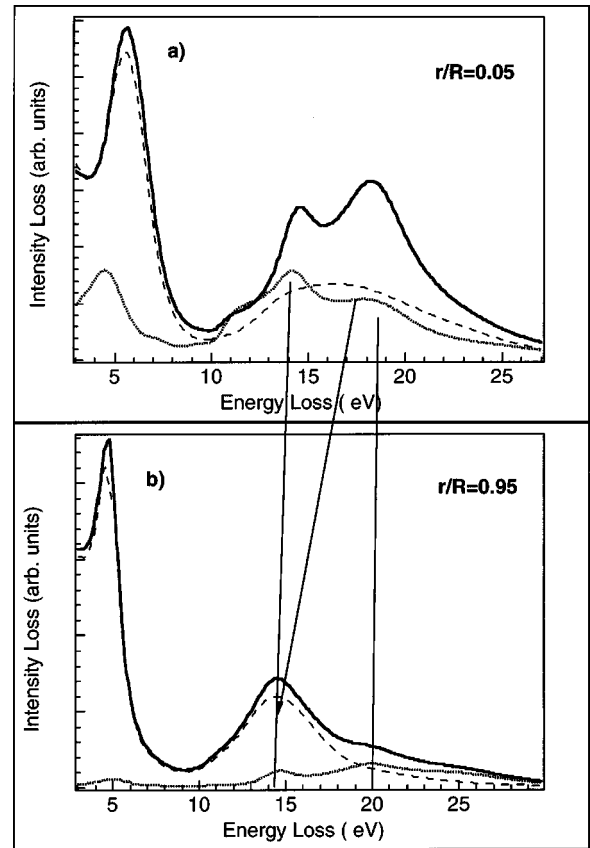
FIG. 5. (a) Simulated EELS spectrum of a C nanotube with a vanishing cavity ($r/R = 0.05$) and large wall thickness (solid line). Dotted line: spectrum obtained for the same nanotube when exciting only the parallel component of the graphite dielectric tensor ($\varepsilon_\perp = 1$). Dashed line: spectrum obtained for the same nanotube when exciting only the perpendicular component of the graphite dielectric tensor ($\varepsilon_\parallel = 1$). (b) Same spectra for a nanotube with a vanishing wall thickness and large cavity ($r/R = 0.95$).

and then is very similar to the $r/R = 0.85$ simulated spectrum. We want to emphasize here the striking result that the r/R dependency of the dielectric response of nanotubes still remains for monoatomic wall nanotubes.

From this collection of simulated and experimental data and from previous work,[4,12,23] two regimes can be distinguished: a first one for $0 < r/R < 0.6$ where spectra show little variation as a function of r/R (see, mainly, Refs. 4 and 23) and a second one for $0.6 < r/R < 1$, where a rapid evolution of the spectra is observed. These two regimes, respectively, correspond to regimes of weak and strong coupling between surface plasmons excited on both internal and external surfaces of the nanotube.

Features in the EELS spectrum from MWCNTs with small r/R values ($r/R < 0.5$) have been interpreted elsewhere.[9] The important idea to be recalled is that for these r/R values, each observed surface-plasmon mode (at 14–15 and 17 eV) possesses a complex character involving both components of the dielectric tensor of the bulk lamellar material. In other words, both modes involve a mixing of in-plane (related to $\varepsilon_\perp$) and out-of-plane (related to $\varepsilon_\parallel$) excitations of the electron gas. This mixing in the dielectric

excitations is illustrated in Fig. 5(a). Together with the EELS simulated spectrum are shown two curves corresponding to two situations where $\varepsilon_\perp$ and $\varepsilon_\parallel$ have successively been set to 1. This corresponds to assume that the nanoparticle is locally transparent (i.e., does not get polarized) along the direction perpendicular (respectively, parallel) to the local anisotropy axis, and therefore an incident radiation can excite only transitions implying the parallel (respectively, perpendicular) component of the dielectric tensor. From Fig. 5(a) it can be seen that the contributions of both component curves cannot be separated, which evidences the mixed character of the surface modes.

Finally, we mention that this series of experiments validates the theoretical predictions of the dielectric model that the relevant parameter is the r/R ratio rather than the absolute values r and R.[4,5,23] Further discussion on that point can be found in Ref. 11 (more precisely, it is shown that in our scattering geometry, for $R < 20$ nm, negligible variations in the spectrum are expected as a function of R).

C. Dielectric response of a SWCNT

We now focus on the strong-coupling regime of the surface plasmons of hollow anisotropic cylinders and more specifically on the $r/R \rightarrow 1$ limit. In this regime, we have already noted the existence of two surface modes at 15 and 19 eV, respectively (the highest one vanishing significantly in intensity) [Figs. 3(a) and 5(b)]. The simulation in Fig. 5(b) also shows a decoupling of in-plane and out-of-plane excitations (contrary to small r/R ratio values for which a decomposition of the spectrum into two components of pure character is impossible). The 15 eV can be exclusively associated with the in-plane component of the dielectric tensor while the 19-eV mode noticeably implies the out-of-plane component only. Such a splitting of the anisotropic electron-gas response into pure in-plane and pure out-of-plane responses, as a result of electrostatic surface coupling, has already been studied for WS_2 nanotubes.[12] Moreover, the lowest-energy mode can be shown to correspond to a tangential mode (with field lines parallel to the surfaces of the nanotube) while the highest-energy mode is a radial mode (the field lines are perpendicular to the surfaces).[12] The radial and tangential modes in a cylinder are, respectively, the counterparts of the antisymmetric and symmetric modes in a slab. In Ref. 12, the tangential mode was related to a maximum of $Im(\varepsilon_\perp)$, while the radial mode corresponded to the bulk plasmon energy of the out-of-plane dielectric constant [defined by the simultaneous conditions $Re(\varepsilon_\parallel) = 0$ with a positive slope and a small value of $Im(\varepsilon_\parallel)$]. This correspondence is even more evident for carbon nanotubes, due to the stronger anisotropic character of the dielectric tensor of graphite. From Fig. 2, we notice that the energy position of the 15 eV mode coincides with the energy $\omega_{0,\perp}$ of the maximum of $Im(\varepsilon_\perp)$, while the energy position of the 19 eV mode is very close to that of the bulk plasmon in the $\varepsilon_\parallel$ component ($\omega_{p,\parallel}$). Moreover, the decrease

in intensity of the highest-energy mode (19 eV) can be understood as follows: the intensity of the radial mode, namely, the intensity of the response with a field perpendicular to the surfaces, is all the weaker as the wall thickness becomes smaller.[24] The single mode of SWCNTs centered at 15 eV, can then be described within the framework of the dielectric model as the limiting case when the radial mode vanishes and the tangential mode only remains.

This points out the surprising result that the continuum dielectric model remains relevant even for a monoatomic layer object. As a matter of fact, this is a consequence of the strong anisotropic character of the graphene sheet and of the graphite stacking. The dielectric response of bulk graphite should differ from that of graphene as a consequence of the weak van der Waals interaction between adjacent graphene atomic layers. To explain our results, we can point out that the out-of-plane excitation, which should be more sensitive to interlayer coupling, vanishes in the case of SWCNTs since the radial mode vanishes. Thus the dielectric response of the SWCNT is mainly driven by the in-plane response of the graphene sheet through $Im(\varepsilon_\perp)$, which is expected to be nearly independent of the presence of the adjacent sheets and therefore is quite similar to that of graphite.[25] Further calculation of the electron states in SWCNTs is required to confirm these simple arguments and extend them to the interpretation of the optical properties.

IV. CONCLUSION

Spatially resolved EELS measurements in a near-field geometry in a STEM can be used to measure the dielectric response of individual SWCNTs. We have demonstrated that this response can be understood by accounting for the strong-coupling limit of surface plasmons in thin MWCNTs. Indeed, the single observed mode centered at 15 eV can be interpreted as the remanence of a tangential (antisymmetric) mode while the radial (symmetric) mode disappears for vanishing wall thickness. We therefore validate one of the major predictions of the dielectric theory, i.e., the r/R ratio dependence of the energy position of the surface-plasmon excitations in hollow nanoparticles. We have shown that the notion of dielectric continuum remains relevant for the description of such a monoatomic layer object.

*Corresponding author.

[1] S. I. Bozhevolnyi, J. Erland, K. Leosson, P. M. W. Skovgaard, and J. M. Hvam, Phys. Rev. Lett. **86**, 3008 (2001).

[2] S. C. Kitson, W. L. Barnes, and J. R. Sambles, Phys. Rev. Lett. **77**, 2670 (1996).

[3] T. R. Jensen, M. L. Duval, K. L. Kelly, A. A. Lazarides, G. C. Schatz, and R. P. Van Duyne, J. Phys. Chem. **103**, 9846 (1999).

[4] A. A. Lucas, L. Henrard, and P. Lambin, Phys. Rev. B **49**, 2888 (1994).

[5] L. Henrard, A. A. Lucas, and P. Lambin, Astrophys. J. **406**, 92 (1993).

[6] L. Henrard, F. Malengreau, P. Rudolf, K. Hevesi, R. Caudano, P. Lambin, and T. Cabioc'h, Phys. Rev. B **59**, 5832 (1999).

[7] G. F. Bertsch, H. Esbensen, and B. W. Reed, Phys. Rev. B **58**, 14 031 (1998).

[8] Z. L. Wang, Micron **27**, 265 (1996).

[9] M. Kociak, L. Henrard, O. Stéphan, K. Suenaga, and C. Colliex, Phys. Rev. B **61**, 13 936 (2000).

[10] T. Stockli, J. M. Bonard, A. Chatelain, Z. L. Wang, and P. Stadelmann, Phys. Rev. B **61**, 5751 (2000).

[11] D. Taverna, M. Kociak, V. Charbois, and L. Henrard, Phys. Rev. B (to be published).

[12] M. Kociak, O. Stéphan, L. Henrard, V. Charbois, R. Tenne, and C. Colliex, Phys. Rev. Lett. **87**, 075501 (2001).

[13] H. Cohen, T. Maniv, R. Tenne, Y. R. Hacohen, O. Stéphan, and C. Colliex, Phys. Rev. Lett. **80**, 782 (1998).

[14] T. Stöckli, Ph.D. thesis, École Polytechnique Fédérale de Lausanne, 1998.

[15] B. W. Reed and M. Sarikaya, Phys. Rev. B **64**, 195404 (2001).

[16] C. Journet, W. K. Maser, P. Bernier, A. Loiseau, M. L. de la Chapelle, S. Lefrant, P. Deniard, R. Lee, and J. E. Fischer, Nature (London) **388**, 756 (1997).

[17] A. Peigney, C. Laurent, and A. Rousset, J. Mater. Chem. **9**, 1167 (1999).

[18] P. Ballongue and M. Tencé (unpublished).

[19] C. Mory and C. Colliex, J. Microsc. Spectrosc. Electron. **10**, A27 (1985).

[20] C. Colliex, M. Tencé, E. Lefèvre, C. Mory, H. Gu, D. Bouchet, and C. Jeanguillaume, Mikrochim. Acta **114−115**, 71 (1994).

[21] C. Jeanguillaume and C. Colliex, Ultramicroscopy **28**, 252 (1989).

[22] B. T. Draine, Astrophys. J. **333**, 848 (1988).

[23] L. Henrard and P. Lambin, J. Phys. B **29**, 5127 (1996).

[24] P. Lambin, A. A. Lucas, and J. P. Vigneron, Phys. Rev. B **46**, 1794 (1992).

[25] A. G. Marinopoulos, L. Reinig, V. Olevano, A. Rubio, T. Phichler, X. Liu, M. Knupfer, and J. Fink, Phys. Rev. Lett. **89**, 076402 (2002).